Available online at www.sciencedirect.com

ScienceDirect

Advances in Space Research 66 (2020) 546–562

ADVANCES IN SPACE RESEARCH (a COSPAR publication)

www.elsevier.com/locate/asr

Assessment of the capabilities and applicability of ionospheric perturbation indices provided in Europe

Claudia Borries [a,*], Volker Wilken [a], Knut Stanley Jacobsen [b], Alberto García-Rigo [c,d], Beata Dziak-Jankowska [e], Guram Kervalishvili [f], Norbert Jakowski [a], Ioanna Tsagouri [g], Manuel Hernández-Pajares [c,d], Arthur A. Ferreira [a], Mainul M. Hoque [a]

[a] German Aerospace Center, Neustrelitz, Germany
[b] Norwegian Mapping Authority, Hønefoss, Norway
[c] UPC-IonSAT, Technical University of Catalonia – BarcelonTech, Barcelona, Spain
[d] Institute of Space Studies of Catalonia (IEEC), Barcelona, Spain
[e] Space Research Center, Polish Academy of Science, Warsaw, Poland
[f] GFZ German Research Centre for Geosciences, Potsdam, Germany
[g] National Observatory of Athens, Athens, Greece

Received 11 February 2020; received in revised form 6 April 2020; accepted 8 April 2020
Available online 22 April 2020

Abstract

Perturbations in the ionosphere are of great interest not only for scientific research, but also for applications using transionospheric radiosignals (e.g. GNSS applications and HF communication), because the transmission of radiosignals is sensitive to the electron density in the ionosphere. However, ionospheric perturbations have manifold character. Their spatial range can vary between global and very local effects (a few hundreds of km range) and their temporal range varies between seconds and days. All these perturbations have different physical background and different impact on applications. Many ionosphere perturbation indices that characterize the state of ionospheric perturbations have been introduced in the past (e.g. ROTI, S4, σ_{Phi}, AATR, R_{eff}, W-index, SISTED, SOLERA, DIXSG, IBI, Dfu/Dfl, etc.). This manuscript is an assessment of a subset of diverse ionospheric indices developed and/or applied in Europe. It describes the objectives of the indices, demonstrates their character in a case study for September 2017, indicates their applicability for different use cases in science and industry and guides users to find the appropriate index for their purposes.

Keywords: Ionosphere; Perturbation; Index; Scales

1. Introduction and objectives

Because the propagation of radiowaves is significantly impacted by the ionosphere, it is essential to monitor and predict perturbations of the ionosphere. This can be done either by the monitoring of ionospheric parameters like the Total Electron Content (TEC) or the *foF*2, or by the monitoring of appropriate ionosphere disturbance indices that describe the degree of perturbation in the ionosphere electron density. An ionospheric index is considered to be a proxy of the complex behaviour of more or less specified perturbation in the ionosphere to improve customer decisions and algorithms. Next to reducing complex perturbations (e.g. ionosphere plasma bubbles) to single values, it is a pragmatic solution to overcome knowledge gaps. Ionosphere perturbation indices can be directly used to estimate the risk in specific application areas and could be used as

* Corresponding author.
E-mail address: claudia.borries@dlr.de (C. Borries).

https://doi.org/10.1016/j.asr.2020.04.013
0273-1177/

Nomenclature

Acronym

AATR Along Arc TEC Rate
AE Auroral Electrojet
AI Activity Index
BNC BKG NTRIP Client
BOM Bureau Of Meteorology
CIRs Co-rotating Interaction Regions
CMEs Coronal Mass Ejections
COSMIC Constellation Observing System for Meteorology, Ionosphere, and Climate
COSPAR Committee on Space Research
dGEC temporal derivative of GEC
Dfl DfoF2-lower
Dfu DfoF2-upper
DIAS Digital Upper Atmosphere Server
DIX Disturbance Ionosphere indeX
DIXSG Disturbance IndeX Spatial Gradient
$DIXSG_p$ planetary DIXSG
Dst Disturbance Storm Time Index
EGNOS European Geostationary Overlay System
EPIs Equatorial Plasma Irregularities
EPBs Equatorial Plasma Bubbles
ESA European Space Agency
ESSP European Satellite Service Provider
EUV Extreme UltraViolet
*foF*2 critical frequency of the F2-layer
GALILEO European Global Navigation Satellite System
GBAS Ground-Based Augmentation Systems
GEC Global Electron Content
GIC Ground Induced Current
GIX Gradient Ionosphere indeX
GLONASS GLObal NAvigation Satellite System
GNSS Global Navigation Satellite System
GPS Global Positioning System
GSFLAI GNSS Solar Flare Activity Indicator
HF High Frequency
IBI Ionospheric Bubble Index
ICAO International Civil Aviation Organisation
IE IMAGE Electrojet index
IMF Interplanetary Magnetic Field
IPPs Ionosphere Pierce Points
LoL Loss-of-Lock
LSTIDs Large-Scale TIDs
MSTIDs Medium-Scale Travelling Ionospheric Disturbances
MUF Maximum Usable Frequency
*NmF*2 maximum electron density of the F2-layer
NOAA National Oceanic and Atmospheric Administration
N-RTK Network Real-Time Kinematic
NTRIP Networked Transport of RTCM via Internet Protocol
PCA Polar Cap Absorption
PPP Precise Point Positioning
R12 12-month running-mean sunspot number
RMS Root Mean Square
ROTI Rate of Change of TEC Index
RTCM Radio Technical Commission for Maritime Services
RTK Real-Time Kinematic
SBAS Space Based Augmentation System
SEP Solar Energetic Particles
SIDC Solar Influence Data Center
SIDX Sudden Ionospheric Disturbance indeX
SISTED Sunlit Ionosphere Sudden TEC Enhancement Detector
SOLERA SOLar Euv flux RAte GNSS proxy
SPEs Solar Protons Events
SPP Single Point Positioning
SRBs Solar Radio Bursts
SRMTID Single Receiver Medium Scale Travelling Ionospheric Disturbance
SSA Space Situational Awareness
SSMTID Single Satellite Medium Scale Travelling Ionospheric Disturbance
TEC Total Electron Content
TIDs Travelling Ionospheric Disturbances
UT Universal Time
WAAS Wide Area Augmentation System

inputs for application specific algorithms. They are especially recommended to be used by non-scientific users, who do not require to assess the physical measures of the ionosphere.

The most intense perturbations are large-scale deviations of TEC from quiet conditions (positive and negative ionosphere storms), significant sharp gradients in TEC and small scale ionosphere irregularities (scintillations). They can cause Loss-of-Lock (LoL) in Global Navigation Satellite System (GNSS) applications, hazardous misleading information during an aircraft approach and landing operations at an airport and wrong ionosphere corrections in single-frequency navigation applications. Ionosphere perturbations with smaller amplitudes like the Medium-Scale Travelling Ionospheric Disturbances (MSTIDs), which are signatures of atmospheric waves, can also have significant impact on applications, especially in the generation of ionosphere corrections in Network Real-Time Kinematic (N-RTK) applications, High Frequency (HF) propagation and geolocation.

In the last decades, numerous ionosphere indices detecting ionosphere perturbations have been published in scientific journals and conferences. However, it is challenging to get an overview on the objectives, capabilities and character of existing ionosphere indices. Therefore, this paper reviews the landscape of multiple ionosphere perturbation indices existing in Europe and provides information about their application. This paper also presents numerous use cases, where ionosphere perturbations are impacting user applications and provides recommendations on ionosphere perturbation indices applicable for these use cases. The goal of this indices review is the homogeneous presentation of a representative set of ionosphere indices and use cases. The intention is to guide users through the landscape of ionosphere indices, but there is no intention to highlight a specific index. The decision about the best applicable index is left to the user, because it often depends not only on specific requirements but also on hardware. However, information on capabilities and limitations of each index will guide the user to find the most-applicable index for the specific purpose.

The need for this assessment did arise from the development of the European Space Agency (ESA) Space Situational Awareness (SSA) Space Weather Network. This review has been generated by the teams involved in the ESA Expert Service Centre for ionosphere weather to support the ESA SSA space weather service developments and also other space weather centers.

2. Description of selected indices

2.1. Rationale of indices selection

The indices used in this assessment are well known. They are based on ionosphere measurements provided by European entities. Of course, there also exists a number of indices based on magnetometer measurements, which also correlate well with ionosphere perturbations. But, these will not be included in this assessment, because our focus are ionosphere perturbations and magnetosphere measurements are ”only” indirect indicators. The considered ionosphere indices are briefly described with their objectives in the following subsections. References are provided to study more details about parametrisation and limitations of these indices.

2.2. AATR

The Along Arc TEC Rate (AATR) index is useful for identifying disturbed periods affecting performance for GNSS users, at regional level. AATR can be easily computed from dual-frequency GNSS measurements. From a devoted analysis of the European Geostationary Overlay System (EGNOS) performances in different ionospheric conditions, it follows that the AATR indicator is able to predict user availability anomalies in a Space Based Augmentation System (SBAS), linked to the ionosphere (Juan et al., 2018).

2.3. Dfu, Dfl

The DfoF2-upper (Dfu) and DfoF2-lower (Dfl) indices were introduced to monitor the ionospheric disturbances at mid-latitudes worldwide (Tsagouri et al., 2000). They are derived from ionosonde measurements and designed to capture the relative deviations of the observed *foF2* from monthly medians. Dfu tends to record positive ionospheric disturbances, while Dfl tends to refer to negative deviations. In principle, the inspection of the two indices can provide information concerning the maximum intensity of the ionospheric storm effects at middle latitudes. The two indices can also support correlation studies of the ionospheric activity with global magnetospheric and geomagnetic activity indices, e.g. Auroral Electrojet (*AE*) and Disturbance Storm Time Index (*Dst*).

2.4. DIXSG, $DIXSG_p$

The Disturbance IndeX Spatial Gradient (DIXSG) is a robust index, which is easy to calculate from GNSS measurements. DIXSG is able to properly characterize temporal and spatial ionospheric variations of small to medium scales. It is designed to serve as model input and to help establishing an ionospheric disturbance scale (Wilken et al., 2018). The DIXSG ($DIXSG_p$) provides a single number for the global ionosphere perturbation condition.

2.5. GEC, dGEC

The Global Electron Content (GEC) index accounts for the complete number of electrons in the global ionosphere for a given epoch. GEC-rate corresponds to its temporal derivative and is rather sensitive for perturbations. Both are global ionospheric indices (Afraimovich et al., 2008; Hernández-Pajares et al., 2009). GEC and the GEC (dGEC) have a high potential to correlate with geomagnetic indices.

2.6. IBI

The Equatorial Plasma Irregularities (EPIs), often referred to as Equatorial Plasma Bubbles (EPBs), are an intrinsic regular phenomenon in the low-latitude post-sunset ionosphere that leaves severe plasma density gradients and magnetic field variations and causes GNSS signal degradations. ESA’s Earth observation constellation mission Swarm provides a regular Level-2 data product called the Ionospheric Bubble Index (IBI). By combining Swarm electron density and magnetic field observations along the orbit track, IBI provides information on ionosphere bubble climatology as well as on the disturbance level of magnetic field data (Park et al., 2013).

2.7. IG, IG12

The IG index is an ionosonde derived index of solar activity. It is a confirmed alternative to the sunspot number (R), leading to more accurate *foF*2 predictions (Liu et al., 1983). In correspondence to the 12-month running-mean sunspot number (R12), the IG12 is the 12-month running-mean of the ionospheric IG index. In its first publication (Liu et al., 1983), the IG index was referred to as the "Global Effective Sunspot Number".

2.8. $R12_{eff}$

The effective Sunspot Number $R1_{eff}$ also belongs to the group of "effective" indices that are based on the use of models and experimental ionospheric data. $R12_{eff}$ has been developed as a model-oriented index (Houminer et al., 1993) to substitute the R12 in ionospheric mapping applications. Today $R12_{eff}$ is applied in models used in the Digital Upper Atmosphere Server (DIAS) system (http://dias.space.noa.gr) to provide European nowcasting *foF*2 maps. DIAS-$R12_{eff}$ has been independently validated as an ionospheric activity index (Tsagouri et al., 2010) that can potentially quantify the level of the ionospheric activity at local and regional scales for scientific and operational purposes.

2.9. ROTI, ROTI@ground

The Rate of Change of TEC Index (ROTI) is a commonly used measure of ionospheric irregularities level. ROTI, as defined in Pi et al. (1997), can be used as a GNSS-based index that characterizes the severity of GNSS phase fluctuations, detects the presence of ionospheric irregularities and measures the irregular structures of TEC spatial gradient. ROTI maps can be applied to monitor and study instantaneous global activity of ionospheric irregularities. Often, ROTI is used as an indicator for phase scintillations, which are measured with the scintillation index σ_ϕ (see Section 2.10). Since phase scintillations at high latitudes are associated with particle precipitation and plasma patches (Jin et al., 2017, 2014; van der Meeren et al., 2015; Clausen et al., 2016), enhanced values of the ROTI index can be associated to them, too. These phenomena occur during geomagnetic storm periods. As the particle precipitation creates aurora, and is often a part of large current systems, ROTI will often coincide with bright auroras and magnetic field disturbances.

Although the algorithm to calculate ROTI is easily implemented, and is common in all publications, there are differences in the individual implementations concerning the choice of the sampling rate of the GNSS data and the time interval over which a value of ROTI is calculated. This impacts the magnitude of ROT and its sensitivity to ionosphere perturbations. This must be taken into account when ROTI values from different studies are going to be compared (Jacobsen, 2014).

On needs to consider that the GNSS satellites are not directly overhead, but distributed in some kind of oval shape around the receivers. Therefore, users at the ground should not refer to a ROTI value at their coordinate from a map of ROTI at ionospheric altitude, because also surrounding ionosphere perturbations will impact their application. A more directly relevant measure for a user at the ground is the ROTI@ground, which is the average value of ROTI observed by a receiver on the ground (average over the set of observed satellites at a given time, c.f. Jacobsen and Andalsvik, 2016).

2.10. Scintillation indices S4 and σ_ϕ

Rapid and intense fluctuations of the amplitude and phase of trans-ionospheric radio signals transmitted by GNSS, including the Global Positioning System (GPS), the GLObal NAvigation Satellite System (GLONASS), and the European Global Navigation Satellite System (GALILEO), is called radio scintillation. This phenomenon, which is usually caused by small-scale irregularities of the ionospheric plasma, can strongly disturb or disrupt the signal transmission. For technical applications, it is useful to apply the well-accepted S4 index describing the amplitude/intensity fluctuation of a received signal (Marques et al., 2018; Hlubek et al., 2014). The scintillation index S4 defines a statistical index to characterize scintillation of the signal amplitude, which are predominant in equatorial areas (Kintner et al., 2007; Hlubek et al., 2014).

The scintillation index σ_ϕ describes the phase fluctuation of a received radio signal. Phase scintillations are typically produced by ionospheric irregularities at small wave numbers and near the first Fresnel radius (Kintner et al., 2007). In general, σ_ϕ is a measure of phase noise due to ionospheric effects (Forte and Radicella, 2002; Forte, 2005; Beach, 2006; Kintner et al., 2007). Please note that this index is hardware dependent. Also, it is sensitive to how data is detrended, which may admit receiver clock noise or GPS satellite motion (Forte and Radicella, 2002).

2.11. SIDX, GIX

Based on the original Disturbance Ionosphere indeX (DIX) approach (Jakowski et al., 2012), spatial and temporal variations of TEC have been separated by the Sudden Ionospheric Disturbance indeX (SIDX) and the Gradient Ionosphere indeX (GIX) (Jakowski and Hoque, 2019) to better understand originating perturbation sources and to react adequately in applications that are sensitive to TEC variations. The indices are well suited to provide an instantaneous, i.e. actual image of temporal and spatial variations of TEC in a well specified area (e.g. ionosphere region impacting a single GNSS station or larger), without taking into account previous measurements. Computations may be performed at each measurement epoch (e.g. every second) or may be averaged over longer time periods.

2.12. SOLERA, SOLERA-drift and SISTED

The SOLar Euv flux RAte GNSS proxy (SOLERA), which was formerly introduced as GSFLA, is a proxy of solar flare Activity Indicator (GSFLAI), photon flux rate based on the sudden response of the ionospheric electron content to solar flare activity (Hernández-Pajares et al., 2012). It gives a direct measure of the geoeffectiveness intensity of solar flares. SOLERA is correlated to the scale of solar flare intensity and has been calibrated vs. it, based on solar X-flux rate. This calibration takes into account the EUV flux extinction factor in the solar atmosphere, which depends on the distance of the flare location to the solar disc center. In addition, SOLERA-drift is calculated to provide detection and warning of solar flares.

The Sunlit Ionosphere Sudden TEC Enhancement Detector (SISTED) is monitoring simultaneous sudden enhancements in the ionospheric TEC at Ionosphere Pierce Points (IPPs) using the drift rate (second difference in time) of the carrier-phase ionospheric combination (LI), which can be derived from GNSS signals gathered in real-time from permanent receivers distributed world-wide by means of Networked Transport of RTCM via Internet Protocol (NTRIP) and BKG NTRIP Client (BNC) (Weber et al., 2016). Generalized sudden enhancements in the sunlit area by SISTED are directly associated to solar flares facing the Earth (García-Rigo, 2012; García-Rigo et al., 2007).

2.13. SRMTID, SSMTID

The Single Receiver Medium Scale Travelling Ionospheric Disturbance (SRMTID) index and the Single Satellite Medium Scale Travelling Ionospheric Disturbance (SSMTID) index indicate in real-time MSTIDs activity for mid latitude stations, without the need of a local network (Hernández-Pajares et al., 2006). It is straightforward to compute as long as the user can derive its receiver's slant TEC values from a set of satellites in view.

2.14. W-index

Similar to geomagnetic k-indices, the ionospheric weather (W) index was introduced for indexing the ionosphere variability (Gulyaeva et al., 2008, 2013; Stanislawska and Gulyaeva, 2015). It can be derived from ionosonde and GNSS measurements. W-index describes positive and negative deviation of ionospheric parameters like the $NmF2$, TEC and $foF2$ from a quiet background in a logarithmic measure. The decimal logarithm of the hourly value of the ionospheric parameter, normalized by the quiet reference (running daily-hourly 27 days median), is taken as a measure of the parameter's variability. Index $W = \pm 1$ is used for the quiet state, $W = \pm 2$ for the moderate disturbance, $W = \pm 3$ for the ionospheric storm, and $W = \pm 4$ for the extreme or anomalous conditions.

3. Index classification and character during the case study of September 2017

According to their purpose and data basis, the presented ionospheric indices differ significantly in their spatial and temporal resolution. There are global indices, indices relevant for Europe, indices with low spatial horizontal resolution (1000 km) and indices with high spatial horizontal resolution (100 km). A few indices are derived per ground station. Here, the spatial resolution would depend on the receiver density. For IBI and SSMTID the definition of spatial resolution is not straight forward, because SSMTID is indicated at the IPPs and IBI is bound to the Swarm satellite orbits. Also a few indices can be calculated for different spatial and temporal resolution. The temporal resolution of the indices data varies between 1 month and 1 s. Table 1 presents an overview of the most common implementations of spatial and temporal resolution of the different indices.

To illustrate the character of the different ionosphere perturbation indices, we choose to show their magnitude in an example case study during 6–9 September 2017, which is a period during one of the most recent major space weather events. Fig. 1 shows the solar and geomagnetic background conditions. This event raised high attention in the scientific and user community. E.g. the journal Space Weather published a special issue reporting about this event. According to the GOES flare alert provided by the Solar Influence Data Center (SIDC), there were 12 solar X- and M-class X-ray flares reported in this period. The peak time of X-class flares was on 6 September 2017, 09:10 UT (X2.2), 12:02 UT (X9.3) and on 7 September, 14:36 UT (X1.3). A geomagnetic storm started on 7 September 2017 around 21 UT, when $SYM-H$, which is a 1-min high-resolution equivalent to Dst, started to decrease significantly. Substorm activity is indicated with AE during 4 different periods (6 Sept. 6–18 UT, 7 Sept. 0–15 UT, 7 Sept. 21 UT- 8 Sept. 4 UT and 8 Sept. 12 UT - 9 Sept. 2 UT), which is considered to be a global index, and the IMAGE Electrojet index IE, which is locally measured with magnetometers in Finland and neighbouring countries. At the same time as Dst drops, AE and IE increase significantly, showing substorm activity. The storm main phase was between 7 September 2017, 21 UT and 8 September 2017, 2 UT, when $SYM-H$ decreased continuously and IE was enhanced. Then, the recovery phase started with increasing $SYM-H$ and low values of AE and IE. During the recovery phase, there was a second substorm. It started on 8 September 2017, 12 UT, when $SYM-H$ suddenly drops again and AE and IE increases. The enhancements of AE and IE, which indicate significant solar wind energy transfer into the magnetosphere, lasted until 9 Sep. 2 UT. Then, the recovery phase continued. According to the minimum Dst index of -150 nT, this geomagnetic storm can be classified as intense (Gonzalez et al., 1994, 2011). It was associated to multiple CMEs reaching Earth.

Table 1
Classification of ionospheric indices concerning spatial (horizontal) and temporal resolution according to recent publications.

Temporal resolution	Spatial resolution					
	Global	Regional/ Europe	1000 x 1000 km	100 x 100 km	At receiver location	other
1 month	IG12					
1 day						
1 h	GEC/dGEC, Dfu/Dfl				AATR	
15 min	GEC/dGEC	$R12_{eff}$	W			
5 min				ROTI, ROTI@ground	AATR, SRMTID	SSMTID (at IPPs)
1 min	SOLERA, SISTED, $DIXSG_p$	SIDX, GIX	DIXSG	ROTI, ROTI@ground, DIXSG, S4, σ_ϕ	S4, σ_ϕ	
1 s						IBI (at satellite orbit, $\approx$ 7 km)

Fig. 2 shows a time series for the 6–10 September 2017 for each of the ionosphere perturbation indices, which were introduced in Section 2. For better visualisation and comparability, we group the indices concerning their spatial resolution. The upper two panels show the global indices. The third panel shows the indices covering Europe, the fourth panel the indices covering a large extent of Europe with roughly 1000 km resolution (shown for Scandinavia) and the fifth panel shows the ones with rather fine spatial resolution of 100 km around 60°N and 10°E. The sixth panel presents indices for individual receivers close to 60° N, 10°E and the last panel shows those that are not related to a specific grid.

In Fig. 1, it is visible that *SOLERA-drift* has usually values close to zero. It significantly peaks during times of flares, indicating that the ionosphere responds. For all X- and M-class flares, the peaks in SOLERA-drift exceed the threshold of 0.025 TECU, which is used for the automatic detection of solar flares.

SISTED shows the percentage of IPPs that indicate over-ionisation. Most of the time, the values fluctuate around 50% and a solar flare is assumed in case sunlit-area values are above 74%. During the X- and M-class flares, SISTED indicates simultaneous over-ionization for 90–100% of the analysed IPPs. Finally, all X-class and all M-class solar flares on 6 and 7 September were geoeffective and they were detected by both SISTED and SOLERA-drift indices in near real-time. The flares on 8 and specially on 9 September were not so geoeffective with smaller footprints in both SISTED and SOLERA-drift.

IG12 is constant during this time period because it has a temporal resolution of one month, showing long term changes. This time resolution does not allow analysing the ionosphere response to an individual storm like the one proposed here.

GEC seems to vary slowly in our case study. There is a peak at 3 UT on 8 September 2017 and another slight enhancement at 16 UT the same day. This seems to be the delayed response to times with enhanced auroral activity. The delay seems to be about 3 h.

dGEC indicates strong TEC changes with an increase on 7 September 2017 at 23:30 UT and a decrease afterwards on 8 September 2017 around 03:00 UT. Also on 8 September 2017 around 12:00 UT, dGEC is positive and shows an increase of global TEC.

Dfu and *Dfl* are rather constant with time on the 6 and 7 September 2017. Dfu records positive values to reflect ionization increase during this time interval in a global perspective, while Dfl ranges around zero. At the time of the onset of auroral activity at around 21 UT on 7 September 2017, Dfu starts increasing. This indicates ionosphere perturbations. There is a significant enhancement of Dfu at 11 UT on 8 September 2017. This indicates a positive ionospheric storm. Afterwards, Dfu decreases to around zero values. Dfl decreases almost at the same time as the onset of the main storm (indicated with decreasing $SYM-H$ in Fig. 1) and remains negative until 10 September 2017. This indicates a negative ionospheric storm.

$DIXSG_p$ quiet time values are about 0.3 with only minor fluctuations. $DIXSG_p$ increases significantly during auroral activity, first between 7 September 2017 23 UT and 8 September 2017, 3 UT and second between 8 September 2017 12 and 18 UT. Like for *IE*, the amplitude of $DIXSG_p$ is larger during the first substorm than during the second.

$R12_{eff}$ is clearly positive on the 6 and 7 September 2017. It turns negative on the 8 September 2017 at 6 UT. Thus, $R12_{eff}$ reflects the positive and negative storm conditions during this case study, as recorded by Dfu/Dfl, with one clear exception: it does not reproduce the positive storm on the 8 September 2017 at 11 UT, which is indicated with Dfu. This is due to the different spatial coverage: although there is a positive storm globally, this does not affect Europe.

SIDX indicates clearly the ionosphere response to the strong flares over Europe on September 6, 11:56 UT, and September 7, 10:15 UT. During the storm activity in the

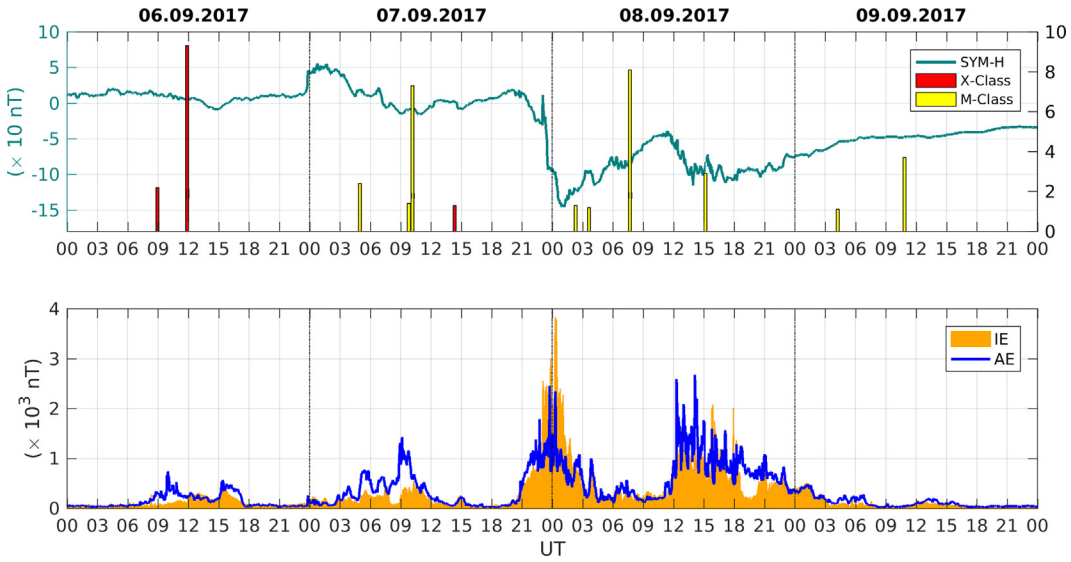

Fig. 1. Geomagnetic conditions during 6–9 September 2017. Upper panel: SYM-H index (blue line). The time of occurrence of solar flares is indicated with bars with colours and size indicating the intensity of the flare. Lower panel: Electrojet Index from IMAGE magnetometers in Finland *IE* (yellow) and Auroral Electrojet Index (AE; blue line).

main phase around midnight on 7/8 September and during a second phase of enhanced activity in the afternoon/evening hours, SIDX fluctuates significantly showing ionosphere perturbations, which are well correlated with substorm activity indicated with *IE* (c.f. Fig. 1).

GIXP± shows only small variations in the course of the storm indicating that horizontal gradients of TEC are not well established during this storm.

W-index initially shows values "+3", indicating a positive deviation of *NmF*2 from monthly median between 15 and 30%. On 6 September a short weak phase of negative W-index equal to "−1". occurred. On 8 September around 19:00 UT, a continuous negative ionospheric storm with W-index = −3 started. It indicates a negative deviation from monthly median up to 15%, which lasted the whole 9 September. The indication of positive and negative storms agrees with Dfu and Dfl index.

ROTI index has a base 'quiet" level above zero. This level may have a slight dependence on constellation (GPS/ GLONASS/ etc.) and receiver equipment, as this is the base noise level in the data (Liu et al., 2019). A typical quiet level is around 1 TECU/min (for ROTI based on 1 s sampling rate data). In our case study, the quiet time ROTI is 0.5 TECU/min on average (c.f. Fig. 2). However, it should be noted that an elevation cut-off of 30 degrees has been applied to the ROTI data to eliminate local effects. This will tend to lower the average ROTI value. ROTI shows no significant peak at the times of the flares on the 6 September. But, ROTI increases significantly during 7 September 2017 23:50 UT to 8 September 2017 03:00 UT and 8 September 2017 12:55 UT to 8 September 2017 15:00 UT, which are times of enhanced auroral electrojet activity (substorms). There occurs an extreme peak of ROTI at exactly 8 September 2017 18:00 UT, when ROTI reaches a value of 9.6 TECU/min. There is no theoretical maximum value of ROTI, but values above 10 TECU/min are rare (for ROTI based on 1 s sampling rate data) and this peak is rather close. There is a peak in *IE* at the same time, but it does not seem to be strong enough to explain the extreme peak in ROTI.

ROTI@ground shows a higher "quiet" level than ROTI. In our case study, it fluctuates around 1 TECU/min. The difference between our ROTI and ROTI@ground values is mainly due to different elevation cut-off angles used. In contrast to ROTI, it shows an obvious peak at the time of the X9.3 flare. The times of enhanced ROTI@ground coincide with times of enhanced ROTI. Also ROTI@ground shows a very strong peak on 8 September 2017 at 18:00 UT.

DIXSG is presented in a scale of 6 activity levels, from 0 (no ionosphere perturbation) to 5 (significant ionosphere perturbations). In general, the DIXSG values agree with the variability of the other indices, like AATR and ROTI, showing increased values during substorm activity. But, there are many peaks in its values, which do not coincide with other indices. It is assumed to be noise.

AATR has a quiet value usually below 0.05 TECU/min. AATR shows a peak on the 6 September 2017 at 12:00 UT, the time of the strong X9.3 flare. AATR increases above 0.1 TECU/min (indicating moderate activity) during 7 September 2017 23:00 UT to 8 September 2017 03:50 UT and 8 September 2017 12:35 UT to 8 September 2017 20:20 UT, which are the times of the substorms with enhanced auroral electrojet activity. However, the amplitudes remain almost entirely below 1 TECU/min, which is considered to be the boundary level between strong and extreme perturbations. But, there occurs one extreme peak of AATR on 8 September 2017 at exactly 17:55

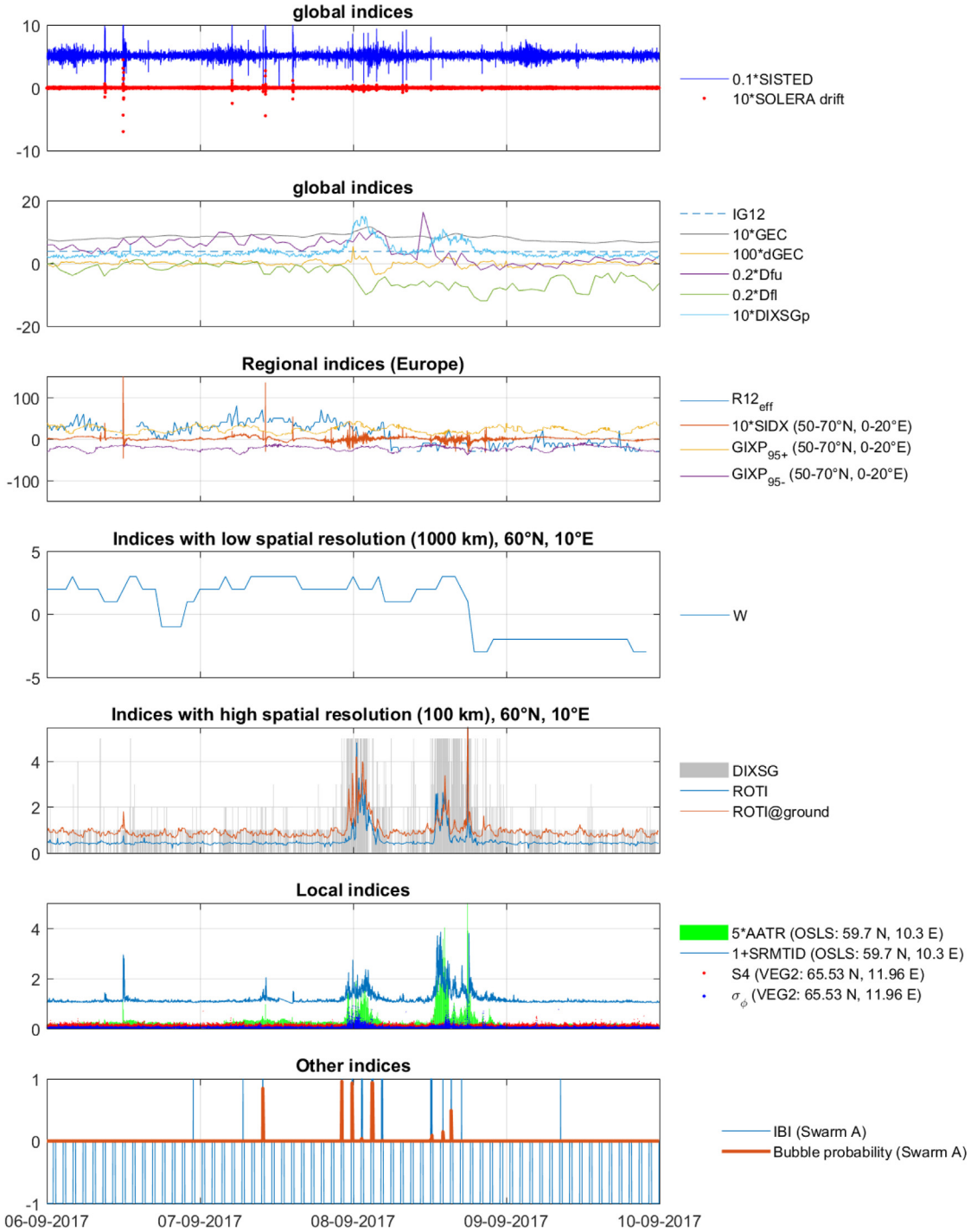

Fig. 2. Characteristics of the ionosphere perturbation indices during the space weather event during 6–9 September 2017. Usually, the shown ionosphere perturbation indices do not have units. AATR, ROTI and ROTI@ground are given in TEC units per minute (TECU/min).

UT. Here, AATR reaches a value of 2.2 TECU/min. The extreme AATR peak at 8 September 2017 close to 18:00 UT coincides with the extreme peak in ROTI.

SRMTID is presented for the same station as AATR. It has quiet values close to zero. They increase and peak at times of solar flares and at times of enhanced auroral activity. The variability is rather similar to AATR.

S4 is fluctuating below 0.2. It does not reach amplitudes above 0.5, which would indicate amplitude scintillation. This agrees with common knowledge, because amplitude scintillations are rare in high latitudes.

σ_ϕ has a quiet time fluctuation below 0.2. The values above 0.5 do irregularly occur during 7 September 2017 23:55 UT to 8 September 2017 01:01 UT and around 8

September 2017 15:00 UT and between 8 September 2017 17:53 UT to 8 September 2017 17:58 UT. This indicates the times when phase scintillations are present. They do overlap with times of enhanced ROTI, DIXSG, DIXSG$_p$ and AATR.

IBI classifies and marks every data point along the Swarm satellite orbit track whether it is affected by EPBs or not. IBI has three values: 0 (quiet data), 1 (data affected by bubbles) and −1 (data are outside the night-time low-latitude range or the quality of the Swarm measurements is poor). There is an additional parameter called "Bubble Probability" that confirms a bubble if it is higher than a certain threshold (e.g. 0.5). If IBI equals 1 and the bubble probability is more than 0.5, the measurements are affected EPBs. Fig. 2 shows an example of IBI and the corresponding bubble probability. There are individual orbits with bubble detection. Considering this storm case study, the bubble occurrence or absence does not seem to be correlated with the storm activity.

In summary, the variety of indices reflect well the complex response of the ionosphere to solar energy input. There are short-term changes like those related to flares and changes with longer duration like the decrease of electron density during the storm recovery phase and multiple intense perturbations of the electron density in high latitudes like scintillations and Travelling Ionospheric Disturbances (TIDs). In general, the indices are rather different in their behaviour, but there are also some indices that show very similar features, like AATR, ROTI and SRMTI.

The ionosphere perturbation indices show us that usually ionosphere perturbations are correlated with solar and geomagnetic perturbations. E.g. all X-class and all M-class solar flares on 6 and 7 September were shown to be geoeffective (as detected with SISTED, SOLERA-drift, SIDX, AATR, etc.). Furthermore, the indices show, that there occurred significant ionosphere perturbations, which are not correlated with solar or geomagnetic measurements, like the perturbation observed on 8 September 2017, 18:00 UT, which is indicated by ROTI and AATR. This intense ionosphere perturbation is not an artefact, because a significant Ground Induced Current (GIC) has been reported at exactly the same time in the same region (Dimmock et al., 2019). The authors did consider this GIC as unusual, because it did not occur in the most geomagnetically active interval. They associated this event to complex rotational and localized features in the ionosphere equivalent currents estimated based on the IMAGE magnetometer measurements.

4. Use cases

4.1. Motivation for use case description

The conditions of the ionosphere are not only of interest for scientific studies but also for technical systems which rely on radio signal transmission. We are describing both natural environment and technical use cases which would benefit from information given by ionospheric indices. As natural environment use cases, we consider natural phenomena, like the perturbations occurring in the ionosphere due to changes of forcing from the Sun (flares, CMEs, etc.) or the lower atmosphere (atmospheric waves). Technical use cases are those when user applications are impacted by perturbations in the ionosphere. Often, technical use cases are related to natural environment use case. If available, the applicable indices will be listed for each use case.

4.2. Natural environment use cases

4.2.1. Ionosphere response to solar flares

Solar flares facing the Earth can produce extra ionization in the ionosphere at the sunlit hemisphere. While X-ray flares impact the D-region and lower E-region of the ionosphere, EUV-flares impact the F-region ionosphere.

The ionosphere indices SOLERA and SISTED (Hernández-Pajares et al., 2012, SOLERA is indicated here as GSFLAI) as well as the ROTI index (with 1 min temporal resolution, Berdermann et al., 2018) and SIDX (Jakowski and Hoque, 2019) are capable to monitor the impact of EUV flares on the ionosphere.

4.2.2. Small-scale irregularities

Small-scale (tens of meters to tens of km) structures in the ionospheric electron density can be caused on the one hand by energetic particle precipitation and plasma instabilities and on the other hand by thermosphere density perturbations/ instabilities. The first effect predominantly occurs in high latitudes (Jacobsen and Dähnn, 2014), while the second effect is common in the equatorial region and causes EPBs (Abdu, 2005). Amplitude and phase scintillation can be estimated with the S4 (e.g. Burke et al., 2003) nd σ_ϕ (e.g. Jacobsen and Andalsvik, 2016) indices respectively. Also, ROTI is commonly used to indicate scintillation effects (Pi et al., 1997) and IBI detects plasma bubbles that have EPIs related signatures in magnetic field observations.

4.2.3. Equatorial plasma bubbles/depletions

EPBs are macro-instabilities observed as structures of depleted plasma density aligned with the magnetic field in the ionosphere F region. The EPBs are a post-sunset geomagnetic equatorial (low latitude) phenomena and they mainly occur at the night-time geomagnetic equatorial/ low latitudes when the ionosphere is unstable due to the steep density gradient in the bottom-side F region. An important information source to better detect and estimate the extent and location of equatorial plasma bubbles are the radio-occultation GNSS measurements from Constellation Observing System for Meteorology, Ionosphere, and Climate (COSMIC) (see for instance Tsai et al., 2016; Dos Santos Prol et al., 2018), and hence the associated scintillation activity. Pradipta and Doherty (2016) determined that EPBs can cause large ionospheric TEC gradients as

follows: (1) steep side walls of the EPBs, and (2) plasma density irregularities inside the bubbles. Navigation systems of satellites and at ground usually suffer from LoL due to scintillations caused by EPBs. Currently, IBI (Park et al., 2013) is a good index indicating the occurrence of EPBs.

4.2.4. Travelling ionospheric disturbances

TIDs are signatures of atmospheric gravity waves in the ionospheric electron density. There are MSTIDs with wavelength between 10 and a few hundreds of km and Large-Scale TIDs (LSTIDs) with wavelength above 1000 km. While MSTIDs originate in the troposphere, LSTIDs originate in the lower thermosphere in the auroral region. Currently, there exist the indices SRMTID/SSMTID (Hernández-Pajares et al., 2017) for the detection of MSTIDs.

4.2.5. Planetary waves

Planetary waves are atmospheric waves with very large zonal extension, which are predominantly of tropospheric origin. They can penetrate (upwards) directly to heights slightly above 100 km and indirectly into the F-region ionosphere. The effects of planetary waves have been observed in the lower ionosphere, in the ionospheric E-region in h'E and sporadic-E (Es) layer and in the F2 region. The corresponding oscillations affect ionospheric predictions on time scales of days. Currently, there does not exist an index indicating planetary wave occurrence.

4.2.6. Strong sharp ionosphere gradients

Large-scale ionospheric spatial gradients are significant changes in the ionosphere electron density which have hundreds of km extension. They can be characterized by the following general parameters: width, slope, velocity. Gradients could potentially pose serious threats to the operation of Ground-Based Augmentation Systems (GBAS) and/or SBAS for GNSS. DIXSG (Wilken et al., 2018) and GIX (Jakowski and Hoque, 2019) have been developed for the detection of ionospheric gradients. Depending on the density of the network, AATR is expected to be able to detect gradients, too.

4.2.7. Ionosphere modelling

Particular empirical models (e.g. used for HF communication prediction) require appropriate ionosphere indices. There exist model-oriented indices, which are developed to work with particular empirical models. They are mean interpolation factors appropriate for specific models, for matching of the model results with the measured ionospheric characteristics at reference stations. It is noted that the correlation between these indices and the ionospheric characteristics are only an evidence of associated phenomena. Very well-known indices of this type are the IG and IG12 index (Liu et al., 1983), developed to be used with the CCIR model. Also, DIAS $R12_{eff}$ (Tsagouri et al., 2005) has been developed for application in modelling.

4.2.8. Deviation from quiet conditions

Ionospheric activity can be characterized by the type (positive or negative) and degree of deviation from the quiet background value. Usually, a deviation of *foF*2 from the running 27-day median larger than 20% is treated as an active state of ionosphere. Positive perturbations have the potential to impact GNSS positioning performance and satellite communication, while negative perturbations are impacting radio-communication at ground and radio signal propagation. W-index (Stanislawska and Gulyaeva, 2015), Dfu/Dfl (Tsagouri et al., 2000) and $R12_{eff}$ are appropriate indices to monitor the deviation from quiet conditions.

4.2.9. Ionosphere perturbations in response to strong solar wind perturbations

Disturbances in the solar wind structure that are observed in the Earth's vicinity perturb significantly the ionosphere-thermosphere system on a global scale, as a result of energy and momentum deposition in geospace environment. The most dramatic effects are related to (i) CMEs that occur most-frequently close to the sunspot maximum and, (ii) Corotating Interaction Regions (CIRs) that are large-scale structures in the heliosphere, which occur predominantly during the declining phase of the solar cycle. The resulting ionosphere-thermosphere effects include a variety of ionospheric disturbances characterized by a wide range of temporal and spatial scales. Small-scale irregularities, LSTIDs, large-scale ionospheric spatial gradients as well as strong deviations of the electron density from quiet conditions can be the response to solar wind and IMF perturbations. Hence, almost all indices (except those indicating flares and MSTIDs) are appropriate for monitoring the ionosphere response to strong solar wind perturbations.

4.2.10. Ionosphere response to solar energetic particles

Solar Energetic Particles (SEP), including protons and electrons, are an important source for ionisation in the high latitude ionosphere in case there is Sun-Earth connection. It needs to be considered that both do not react with the atmosphere equally. Energetic electrons are the main driver of auroral emission and precipitation-induced ionisation in high latitudes. However, sometimes and for some locations, proton precipitation can be a major source of ionization in the auroral ionosphere. During Solar Protons Events (SPEs), the majority of the energy of energetic protons is deposited in the D-region ionosphere (around 50–80 km altitude). This region is frequently used for ionospheric radio communications, because most of the radio signal energy absorption occurs there. Riometers are capable to measure the absorption of radiowaves in the iono-

sphere, but there does not exist an ionosphere index yet, which describes the impact of SEP in the ionosphere.

4.3. Technical system and infrastructure use cases

4.3.1. Space based augmentation system degradation

Wide Area Augmentation System (WAAS) and EGNOS are the American and European examples for SBAS. EGNOS has been designed to improve the navigation accuracy and to protect navigation accuracy dependent applications such as commercial aviation against misleading information. EGNOS performance degradation events can be associated to ionospheric phenomena. The availability of EGNOS corrections has been shown to be correlated with ionospheric indices.

The AATR ionospheric index (Juan et al., 2018) is currently used by the European Satellite Service Provider (ESSP) to study the connection between ionospheric disturbances and impacts on EGNOS availability (and take appropriate actions in case necessary). Also ROTI (Abe et al., 2017a; Abe et al., 2017; Pintor et al., 2015) and the scintillation indices S4 and σ_ϕ (Aquino et al., 2005) have been shown to be useful for SBAS performance studies. The study Béniguel et al. (2017) showed the applicability of S4 and σ_ϕ, AATR, ROTI, SISTED and SRMTID. The application of GIX for EGNOS has been discussed in Jakowski and Hoque (2019). In addition, all other ionosphere indices are supposed to deliver valuable information for SBAS, too.

4.3.2. Lost GNSS signal (loss-of-lock)

GNSS receiver LoL can be caused by different perturbations in the ionosphere. Plasma bubbles causing amplitude scintillations are a common source of LoL in equatorial regions (Aquino et al., 2005; Marques et al., 2018; Liu et al., 2017). All the total loss of GPS signal events encountered by the Swarm satellites at equatorial/low latitudes are related to EPBs (Xiong et al., 2016). The lost number of channels depends on the depletion depth, i.e. the deeper the electron density depletion in the EPBs, the more probable is the LoL in all channels. In addition, Pi et al. (1997) show that LoL may be associated with the strong phase fluctuations, indicating that large phase fluctuations may affect GPS applications. LoL can be also caused by Solar Radio Bursts (SRBs), as shown by e.g. Carrano et al. (2009). However, the impact of SRBs is not related to ionosphere perturbations but the interference of radiowaves.

Appropriate indices indicating the risk of LoL are IBI (Xiong et al., 2016), ROTI (Pi et al., 1997) and S4 (Liu et al., 2017).

4.3.3. Radio communication impact

Representative electron densities associated with various layers in the ionosphere correspond to critical frequencies that fall within the HF band. As a result, the HF band is most sensitive to ionospheric effects (Goodman, 2005). HF communication systems for voice and data missions are typical examples of systems affected by the ionospheric conditions. HF communications have been proven to be the most valuable communication backup systems in case of military and civil protection operations, like natural disasters.

HF waves propagating through the ionosphere may experience reflection, refraction, attenuation and modification of the plane of polarization. Reflection of HF waves occurs depending on their frequency, the degree of ionization of the layers of the ionosphere, and on the angle of propagation.

Space weather impact on HF can be significant. It includes: solar flare induced absorption, Polar Cap Absorption (PCA), angle-of-arrival fluctuations, auroral scatter, multipath distortion, HF radar ranging errors, broadcast coverage variations, storm-driven Maximum Usable Frequency (MUF) variations, and many more.

There is no application of ionosphere indices for radio communication, which is published yet. But, various indices are expected to be applicable: DIAS $R12_{eff}$, Dfu/Dfl, W-index, ROTI, S4, σ_ϕ, SISTED/SOLERA, GEC and SRMTID/SSMTID.

4.3.4. Performance degradation of real-time kinematic

N-RTK positioning services support users by calculating and transmitting information regarding observation biases (e.g. ionospheric delay) to the user. As the processing includes phase measurements, the network processor must solve for phase ambiguities in order to achieve a precise solution. Rapid variations in the phase measurements will affect the processing in several ways, including but not limited to:

- Noise in the estimated values, which will result in noise in the final coordinates;
- Loss of data due to data quality checks in the software;
- Loss of fixed (integer) solutions for phase ambiguities;
- Loss of data due to loss of satellite lock at the network receivers.

Indices applicable to indicate potential performance degradation of N-RTK are those which indicate the level of fluctuations in GNSS observables. Specific examples of such indices are ROTI, ROTI@ground and σ_ϕ (Jacobsen and Andalsvik, 2016). The GNSS positioning errors increase faster-than-linear with ROTI value (Jacobsen and Andalsvik, 2016; Jacobsen and Dähnn, 2014; Jacobsen and Schäfer, 2012). Below 2 TECU/min the impact is small. At 5 TECU/min the positioning error has been observed to reach around 10 times its quiet-ROTI value in studies using high-accuracy positioning, like Precise Point Positioning (PPP) and Real-Time Kinematic (RTK) (Jacobsen and Dähnn, 2014). For positioning applications, where an augmentation system is used (e.g. RTK positioning), the positioning error vs. ROTI graph will

have a breakpoint where the disturbances become strong enough to disrupt the processing in the augmentation system. This has been observed to be at around 3–4 TECU/min for a N-RTK service in Norway (Jacobsen and Schäfer, 2012).

DIXSG and eventually AATR also give measures of these situations. The impact of MSTIDs on precise GPS processing has been studied and demonstrated using SRMTID (Hernández-Pajares et al., 2017).

4.3.5. Degraded positioning accuracy for stationary applications

This use case concerns a measurement campaign spanning from an hour up to several days to establish a very accurate single coordinate. The processing is typically performed in post-processing, allowing the use of external data to generate a better result. While space weather is less of a problem for this use than for dynamic positioning, awareness of space weather conditions can be used to filter or otherwise correct the data. Some applications may even include ionosphere data in the calculations. Sieradzki and Paziewski (2016a) reported the impact of MSTIDs on rapid static positioning. Sieradzki and Paziewski (2016b) reported the impact of intense TEC fluctuations on GNSS positioning, giving an example of a modified algorithm using Rate of TEC (ROT) to mitigate the effects of fluctuations on the positioning.

4.3.6. Degraded positioning accuracy for mobile applications

This use case concerns positioning for a moving object (e.g. car, boat, drone, etc.). These need a rapid position update, with the coordinate changing in time. This kind of positioning is vulnerable to space weather disturbances. Since the calculations are generally performed in real-time, it may not have access to external correction data, and have to base each result on a short time span of measurements. Space weather indices may be used to inform the user if they should trust the results. Alternatively, if the user already has detected a problem, it can inform the user that the source of their problem is the disturbed ionosphere.

The connection between space weather-related GNSS signal disturbances and increased errors in accurate real-time positioning is well known and there exist many publications on the topic. To give some examples: Aquino et al. (2005) showed ionospheric scintillations impacting GNSS users in northern Europe using the σ_ϕ index. Jacobsen (2014) showed how the 3D PPP error correlates with ROTI.

4.3.7. Model degradation in single point positioning

One of the main errors for GNSS signal propagation is the ionospheric delay. In Single Point Positioning (SPP), GNSS broadcast ionospheric models provide an estimate of the ionospheric delay. Klobuchar ionospheric delay model is designed as such a GNSS correction model. This model accounts for at least 50% of Root Mean Square (RMS) error due to the ionospheric propagation effect (Klobuchar, 1987). Recently, Hoque et al. (2018) published a new approach for reducing this error. However, especially during disturbed conditions, the deviations between model and actual ionospheric delay can still impact significantly the performance of SPP.

The W-index can provide an indication for this model degradation, but we like to note that it does not consider any ionospheric delay model and is not a proven estimate.

4.3.8. Ground based augmentation systems

GBAS is a support system based on a small number of GNSS receivers in the vicinity of an airport. Based on the measurements from this local network, corrections are calculated and transmitted to nearby aircrafts to assist them in calculating accurate and reliable positions. The main ionospheric threat to GBAS systems are steep spatial gradients in TEC, as this may cause the conditions at the aircraft to be significantly different from the conditions at the GBAS receiver(s) (Pullen et al., 2009; Jung and Lee, 2012). No study correlating GBAS performance and ionospheric indices has been published yet. However, we suggest the application of DIXSG and GIX, since it has been proven to detect ionosphere gradients. Smaller gradients are generated by TIDs. The impact on GBAS is not known yet. However, we suggest to study the correlation of GBAS performance and MSTIDs indices like SRMTID and SSMTID, too.

4.3.9. Polar cap absorption

PCA describes the effect of complete blocking of all ionospheric radio communication caused by the ionosphere. This type of absorption occurs only in latitudes greater than 62° (geomagnetic). It follows SPEs associated with major solar flares with a delay varying from about 20 min to about 20 h, and last for a few days. It has characteristic diurnal variation which gradually fades out over successive days. The absorption has a maximum value around local noon and a minimum value around local midnight. From the riometer record it is observed that during a typical PCA event, the absorption has a steep onset and increases at a uniform rate for a few hours, levels off at the maximum value for some hours and then slowly begins a smooth recovery lasting a few days. Currently, there is no index available which indicates PCA. However, solar flare indicators like SISTED and SOLERA are suggested to be used as precursors or proxies.

5. Indices applicability

The applicability of ionosphere indices, which has been addressed in the sections before, is presented now in an overview table (Table 2). References are given in the table cells, where the application of an index for a certain use case has been proven in a journal paper. These references are a selection of prominent examples, but are certainly

not a complete list. In addition, recommendations for further application of the listed indices are indicated in Table 2 with asterisks. These recommendations are based on the authors' experience, but they have not been published yet.

This overview table allows a quick assessment of the existence of appropriate ionosphere indices for each use case. It is easy to see that some use cases are well served with indices and other use cases are lacking appropriate indices. There are use cases like SBAS/EGNOS, where all indices can give support for the performance improvement. And there are use cases like planetary waves and SEP where no indices are available yet. It can be argued, that not each use case must be addressed necessarily with an index, e.g. planetary waves. But, since the ionosphere response to SEP can impact significantly communication applications and also GNSS, we recommend the development of appropriate measures and indices, that can help estimating and mitigating the impact.

6. Status and next steps

So far, the assessment comprises 19 ionosphere indices and 20 use cases, providing guidance on which ionosphere index is applicable for which use case. This information is expected to support essentially the planning and development of European space weather information and warning systems like e.g. the ESA SSA Space Weather Portal or the International Civil Aviation Organisation (ICAO) space weather centers. Such space weather service centers can use this information to design, implement and provide warnings and alerts, which are dedicated to specific user needs. In a next step, the centers need to identify those indices, which are applicable for their users and then, if not done already, the operational provision of the indices must be implemented. For the design and implementation of warning messages, it is necessary to statistically assess the impact on applications and define thresholds for issuing warning. It is recommended to identify levels of quite, moderately and strongly disturbed ionosphere. For individual indices like AATR and DIXSG such levels are known and well received. It is important to be careful in the analysis and definition of thresholds for the impact on technical systems, because the ionosphere impact on technical systems may vary dependent on the hardware used.

Also, this assessment of ionosphere indices is a valuable contribution to the international discussion on the generation of ionosphere scales as an ionosphere equivalent to the geomagnetic and radiation scales defined by the United States National Oceanic and Atmospheric Administration (NOAA). In contrast to the existing scales, ionosphere scales cannot rely on only one ionosphere index because of the complexity and manifold of ionosphere perturbations. During space weather impacts (e.g. CMEs), it can occur that ionosphere perturbations and impact on applications are present in one region (e.g. high latitudes) but not in others. The application of indices for the definition of ionosphere scales also needs to consider that some ionosphere perturbations, which impact applications, are regular phenomena and are not related to space weather impact (e.g. scintillations in low latitudes). This discussion is addressed by an international initiative organised in a working group of the Committee on Space Research (COSPAR, https://iswat-cospar.org/g2b-04/).

Since this study focuses on European indices, it does not yet cover all globally available ionosphere indices. On a global level, there are more ionosphere indices like the recently published I-scale (Nishioka et al., 2017), the ionosphere variability index, Vσ (Gulyaeva and Mannucci, 2020), the T-index applied for HF communication at the Australian Bureau Of Meteorology (BOM), the ionospheric Activity Index (AI) (Bremer et al., 2006; Mielich and Bremer, 2010) or the model-oriented RESSN to work with MUF forecast used for HF communication, among others. In the future, it is recommended that this review could be complemented with additional and new ionosphere indices assessment.

7. Summary and conclusions

This review provides an overview of ionosphere indices used and provided in Europe and shows their characteristics during a case study in September 2017. In addition, the application of these indices for the detection of physical processes impacting the ionosphere and ionosphere impact on technical systems is provided. We showed that for most ionosphere perturbations, there exists at least one index for their detection. For some use cases, e.g. EGNOS performance degradation, there even exist manifold indices which can help detecting and mitigating the ionosphere impact. But, there are also some ionosphere perturbations which are not yet described by an index. One can argue that individual ionosphere perturbations, which do not seriously impact technical systems (e.g. planetary wave signatures), do not require a description with an index. Nevertheless, we recommend that at least all ionosphere perturbations seriously impacting technical systems should be detectable with a certain index. In particular, we see a development need for an index for PCA effects.

Often, technical applications need information about multiple kinds of ionosphere perturbations. Therefore, it is worth considering the development of dedicated indicators, which can be the combination of ionosphere perturbation indices which are appropriate for the considered application. Such a combination was proposed e.g. in Jakowski and Hoque (2019) using of SIDX and GIX. Also the ESA Space Weather Portal (http://swe.ssa.esa.int/) provides, with an initial version of a GNSS Performance Indicator, a value-added product that makes use of the combination of different ionosphere indices and measurements (e.g. ROTI) to provide a performance estimation for different GNSS applications.

For the general information about the state of the ionosphere, it is necessary to define ionosphere scales. Here, it is recommended to identify different levels from quiet to

Table 2
Overview on applicable indices for different use cases. References are given for those applications which have been reported in following references: [1] Berdermann et al. (2018),Jakowski and Hoque (2019), [3] Hernández-Pajares et al. (2012) and García-Rigo (2012),Pi et al. (1997), [5] Jacobsen and Andalsvik (2016),Burke et al. (2003), [7] Park et al. (2013),Hernández-Pajares et al. (2017), [9] Wilken et al. (2018), [10] Liu et al. (1983), [11] Tsagouri et al. (2005), [12] Tsagouri et al. (2000), [13] Tsagouri et al. (2010), [14] Stanislawska and Gulyaeva (2015), [15] Juan et al. (2018), [16] Béniguel et al. (2017), [17] Abe et al. (2017a), [18] Abe et al. (2017), [19] Aquino et al. (2005), [20] Xiong et al. (2016), [21] Liu et al. (2017), [22] Sieradzki and Paziewski (2016b), [23] Jacobsen (2014). Recommended applications of indices are indicated with asterisks.

	Use case	AATR	Dfu/ Dfl						DIXSG	GEC	GIX	IBI	IG12	$R12_{eff}$
ROTI	$S4/\sigma_\phi$	SIDX										SISTED/ SOLERA	SRMTID/ SSMTID	W-index
Natural	Solar flares								[1]		[2]	[3]		
	Small scale irregularities						*		[4]	[5, 6]				
	Equatorial plasma depletions						[7]							
	MSTIDs/ LSTIDs												[8]	
	Planetary waves	*												
	TEC gradients			[9]		[2]								
	Ionosphere modelling							[10]	[11]					
	Deviation from quiet conditions		[12]						[13]					[14]
	CME, CIR, etc.	[15]	[12]	[9]	*	*	*		[13]	[4]	[5, 6]	*			[14]
	SEP													
Technical	SBAS/EGNOS	[15, 16]	*	*	*	[2]	*		*	[16, 17, 18]	[16, 19]	[2]	[8]	*	*
	LoL GNSS						[20]			[4]	[21]				
	Radio communication	*	*		*				*	*	*		*	*	*
	RTK performance			*							[5]	[5]		[8]	
	Stationary GNSS application									[22]					
	Mobile GNSS application									[23]	[19]				
	Model degradation (SPP)														*
	GBAS impact			*		*								*	
	Polar Cap Absorption (PCA)										*	*			

extremely disturbed ionosphere. For this purpose, we also recommend the combination of different ionospheric indices. An overall estimation of the ionosphere state is provided by different global ionosphere perturbation indices, which have been presented here (e.g. GEC, dGEC, $DIXSG_p$). However, since the ionosphere conditions usually vary significantly between different regions, the global scales have to be complemented with regional equivalents.

Furthermore, the definition of scales requires the knowledge about thresholds for the detection and classification of ionosphere perturbations. Therefore, it is necessary to continue and strengthen the work on the definition of thresholds.

Finally, this review is meant to be used as a reference document in space weather services and support the planning of development and provision of appropriate ionosphere perturbation alarms for users.

Acknowledgement

We thank ESA for stimulating and supporting this work in the frame of the ESA Space Situation Awareness (SSA) Programme under contract No. 4000113184/15/D/MRP. We also thank the SIDC for providing the solar flare information in the ESA SSA Space Weather Portal (http://swe.ssa.esa.int). Thanks also to the World Data Center Kyoto, who is providing the $SYM-H$ and AE index and the Finnish Meteorological Institute for providing the Auroral Electro Jet from the International Monitor for Auroral Geomagnetic Activity (IMAGE, http://space.fmi.fi/image/). We thank ESA for providing the Swarm Level 2 product IBI (https://earth.esa.int/web/guest/swarm/data-access). We also extend our gratitude to IGS for GNSS data and products provision (Johnston et al., 2017).

References

Abdu, M., 2005. Equatorial ionosphere-thermosphere system: Electrodynamics and irregularities. Adv. Space Res. 35, 771–787.

Abe, O.E., Otero Villamide, X., Paparini, C., Ngaya, R.H., Radicella, S. M., Nava, B., 2017a. Signature of ionospheric irregularities under different geophysical conditions on SBAS performance in the western African low-latitude region. Annales Geophysicae 35, 1–9. https://doi.org/10.5194/angeo-35-1-2017, https://www.ann-geophys.net/35/1/2017/.

Abe, O.E., Paparini, C., Ngaya, R.H., Otero Villamide, X., Radicella, S. M., Nava, B., 2017. The storm-time assessment of GNSS-SBAS performance within low latitude African region using a testbed-like platform. Astrophys. Space Sci. 362, 170. https://doi.org/10.1007/s10509-017-3150-8.

Afraimovich, E.L., Astafyeva, E.I., Oinats, A.V., Yasukevich, Y.V., Zhivetiev, I.V., 2008. Global electron content: a new conception to track solaractivity. Annales Geophysicae 26, 335–344. https://doi.org/10.5194/angeo-26-335-2008.

Aquino, M., Moore, T., Dodson, A., Waugh, S., Souter, J., Rodrigues, F. S., 2005. Implications of ionospheric scintillation for GNSS users in Northern Europe. J. Navig. 58, 241–256. https://doi.org/10.1017/S0373463305003218.

Beach, T.L., 2006. Perils of the GPS phase scintillation index (σ_Φ). Radio Sci. 41, RS5S31. https://doi.org/10.1029/2005RS003356, https://agupubs.onlinelibrary.wiley.com/doi/abs/10.1029/2005RS003356, arXiv: https://agupubs.onlinelibrary.wiley.com/doi/pdf/10.1029/2005RS003356.

Béniguel, Y., Cherniak, I., Garcia-Rigo, A., Hamel, P., Hernández-Pajares, M., Kameni, R., Kashcheyev, A., Krankowski, A., Monnerat, M., Nava, B., Ngaya, H., Orus-Perez, R., Secrétan, H., Sérant, D., Schlüter, S., Wilken, V., 2017. MONITOR Ionospheric Network: two case studies on scintillation and electron content variability. Anna. Geophys. 35, 377–391. https://doi.org/10.5194/angeo-35-377-2017, https://www.ann-geophys.net/35/377/2017/.

Berdermann, J., Kriegel, M., Banyś, D., Heymann, F., Hoque, M.M., Wilken, V., Borries, C., Heßelbarth, A., Jakowski, N., 2018. Ionospheric Response to the X9.3 Flare on 6 September 2017 and Its Implication for Navigation Services Over Europe. Space Weather 16, 1604–1615. https://doi.org/10.1029/2018SW001933, https://agupubs.onlinelibrary.wiley.com/doi/abs/10.1029/2018SW001933, arXiv: https://agupubs.onlinelibrary.wiley.com/doi/pdf/10.1029/2018SW001933.

Bremer, J., Cander, L., Mielich, J., Stamper, R., 2006. Derivation and test of ionospheric activity indices from real-time ionosonde observations in the European region. J. Atmos. Sol.-Terres. Phys. 68, 2075–2090. https://doi.org/10.1016/j.jastp.2006.07.003, http://www.sciencedirect.com/science/article/pii/S1364682606001738.

Burke, W.J., Huang, C.Y., Valladares, C.E., Machuzak, J.S., Gentile, L. C., Sultan, P.J., 2003. Multipoint observations of equatorial plasma bubbles. J. Geophys. Res.: Space Phys., 108 https://doi.org/10.1029/2002JA009382, https://agupubs.onlinelibrary.wiley.com/doi/abs/10.1029/2002JA009382, arXiv: https://agupubs.onlinelibrary.wiley.com/doi/pdf/10.1029/2002JA009382.

Carrano, C.S., Bridgwood, C.T., Groves, K.M., 2009. Impacts of the December 2006 solar radio bursts on the performance of GPS. Radio Sci. (44) https://doi.org/10.1029/2008RS004071, https://agupubs.onlinelibrary.wiley.com/doi/abs/10.1029/2008RS004071, arXiv: https://agupubs.onlinelibrary.wiley.com/doi/pdf/10.1029/2008RS004071.

Clausen, L.B.N., Moen, J.I., Hosokawa, K., Holmes, J.M., 2016. GPS scintillations in the high latitudes during periods of dayside and nightside reconnection. J. Geophys. Res.: Space Phys. 121, 3293–3309. https://doi.org/10.1002/2015JA022199, https://agupubs.onlinelibrary.wiley.com/doi/abs/10.1002/2015JA022199, arXiv: https://agupubs.onlinelibrary.wiley.com/doi/pdf/10.1002/2015JA022199.

Dimmock, A.P., Rosenqvist, L., Hall, J.O., Viljanen, A., Yordanova, E., Honkonen, I., André, M., Sjöberg, E.C., 2019. The GIC and Geomagnetic Response Over Fennoscandia to the 7–8 September 2017 Geomagnetic Storm. Space Weather 17,989–1010. https://doi.org/10.1029/2018SW002132, https://agupubs.onlinelibrary.wiley.com/doi/abs/10.1029/2018SW002132, arXiv:https://agupubs.onlinelibrary.wiley.com/doi/pdf/10.1029/2018SW002132.

Dos Santos Prol, F., Hernández-Pajares, M., Tadeu de Assis Honorato Muella, M., De Oliveira Camargo, P., 2018. Tomographic imaging of ionospheric plasma bubbles based on GNSS and radio occultation measurements. Remote Sens., 10 https://doi.org/10.3390/rs10101529, https://www.mdpi.com/2072-4292/10/10/1529.

Forte, B., 2005. Optimum detrending of raw GPS data for scintillation measurements at auroral latitudes. J. Atmos. Sol.-Terres. Phys. 67, 1100–1109. https://doi.org/10.1016/j.jastp.2005.01.011. http://www.sciencedirect.com/science/article/pii/S136468260500091X. Space weather and RF communications: monitoring and modelling..

Forte, B., Radicella, S.M., 2002. Problems in data treatment for ionospheric scintillation measurements. Radio Sci. 37, 8–1–8–5. https://doi.org/10.1029/2001RS002508. https://agupubs.onlinelibrary.wiley.com/doi/abs/10.1029/2001RS002508, arXiv: https://agupubs.onlinelibrary.wiley.com/doi/pdf/10.1029/2001RS002508..

García-Rigo, A., 2012. Contributions to ionospheric determination with global positioning system: solar flare detection and prediction of global maps of total electron content. Ph.D. thesis. Technical University of Catalonia (UPC).

García-Rigo, A., Hernández-Pajares, M., Juan, J., Sanz, J., 2007. Solar flare detection system based on global positioning system data: First results. Adv. Space Res. 39, 889–895. https://doi.org/10.1016/j.asr.2006.09.031.

Gonzalez, W.D., Echer, E., Tsurutani, B.T., Clúa de Gonzalez, A.L., Lago, A.D., 2011. Interplanetary origin of intense, superintense and

extreme geomagnetic storms. Space Sci. Rev. 158, 69–89. https://doi.org/10.1007/s11214-010-9715-2.

Gonzalez, W.D., Joselyn, J.A., Kamide, Y., Kroehl, H.W., Rostoker, G., Tsurutani, B.T., Vasyliunas, V.M., 1994. What is a geomagnetic storm? J. Geophys. Res.: Space Phys. 99, 5771–5792. https://doi.org/10.1029/93JA02867.

Goodman, J.M., 2005. Space Weather & Telecommunications. The Springer International Series in Engineering and Computer Science. vol.. 782. Springer, US. https://doi.org/10.1007/b102193..

Gulyaeva, T., Arikan, F., Hernandez-Pajares, M., Stanislawska, I., 2013. GIM-TEC adaptive ionospheric weather assessment and forecast system. J. Atmos. Sol.-Terres. Phys. 102, 329–340. https://doi.org/10.1016/j.jastp.2013.06.011. http://www.sciencedirect.com/science/article/pii/S1364682613001879..

Gulyaeva, T.L., Stanislwska, I., Tomasik, M., 2008. Ionospheric weather: cloning missed foF2 observations for derivation of variability index. Ann. Geophys. 26, 315–321. https://www.ann-geophys.net/26/315/2008/, htpps://doi.org/10.5194/angeo-26-315-2008..

Tamara L. Gulyaeva, Anthony J. Mannucci,Echo of ring current storms in the ionosphere,Journal of Atmospheric and Solar[HYPHEN]Terrestrial Physics, 205, 2020, 105300, https://doi.org/10.1016/j.jastp.2020.105300.

Hernández-Pajares, M., García-Rigo, A., Juan, J.M., Sanz, J., Monte, E., Aragón-Angel, A., 2012. GNSS measurement of EUV photons flux rate during strong and mid solar flares. Space Weather 10. https://doi.org/10.1029/2012SW000826. https://agupubs.onlinelibrary.wiley.com/doi/abs/10.1029/2012SW000826, arXiv: https://agupubs.onlinelibrary.wiley.com/doi/pdf/10.1029/2012SW000826..

Hernández-Pajares, M., Juan, J.M., Sanz, J., 2006. Medium-scale traveling ionospheric disturbances affecting GPS measurements: Spatial and temporal analysis. J. Geophys. Res.: Space Phys. 111. https://doi.org/10.1029/2005JA011474. https://agupubs.onlinelibrary.wiley.com/doi/abs/10.1029/2005JA011474, arXiv: https://agupubs.onlinelibrary.wiley.com/doi/pdf/10.1029/2005JA011474..

Hernández-Pajares, M., Juan, J.M., Sanz, J., Orus, R., Garcia-Rigo, A., Feltens, J., Komjathy, A., Schaer, S.C., Krankowski, A., 2009. The IGS VTEC maps: a reliable source of ionospheric information since 1998. J. Geodesy 83, 263–275. https://doi.org/10.1007/s00190-008-0266-1.

Hernández-Pajares, M., Wielgosz, P., Paziewski, J., Krypiak-Gregorczyk, A., Krukowska, M., Stepniak, K., Kaplon, J., Hadas, T., Sosnica, K., Bosy, J., Orus-Perez, R., Monte-Moreno, E., Yang, H., Garcia-Rigo, A., Olivares-Pulido, G., 2017. Direct MSTID mitigation in precise GPS processing. Radio Sci. https://doi.org/10.1002/2016RS006159.2016RS006159.

Hlubek, Nikolai, Berdermann, Jens, Wilken, Volker, Gewies, Stefan, Jakowski, Norbert, Wassaie, Mogese, Damtie, Baylie, 2014. Scintillations of the GPS, GLONASS, and Galileo signals at equatorial latitude. J. Space Weather Space Clim. 4, A22. https://doi.org/10.1051/swsc/2014020..

Hoque, Mohammed Mainul, Jakowski, Norbert, Berdermann, Jens, 2018. Positioning performance of the NTCM model driven by GPS Klobuchar model parameters. J. Space Weather Space Clim. 8, A20. https://doi.org/10.1051/swsc/2018009..

Houminer, Z., Bennett, J., Dyson, P., 1993. Real-time ionospheric model updating. J. Electrical Electron. Eng. Australia 13, 99–104.

Jacobsen, K.S., Schäfer, S., 2012. Observed effects of a geomagnetic storm on an RTK positioning network at high latitudes. J. Space Weather Space Climate 2, A13. https://doi.org/10.1051/swsc/2012013.

Jacobsen, Knut Stanley, 2014. The impact of different sampling rates and calculation time intervals on ROTI values. J. Space Weather Space Clim. 4, A33. https://doi.org/10.1051/swsc/2014031..

Jacobsen, Knut Stanley, Andalsvik, Yngvild Linnea, 2016. Overview of the 2015 St. Patrick's day storm and its consequences for RTK and PPP positioning in Norway. J. Space Weather Space Clim. 6, A9. https://doi.org/10.1051/swsc/2016004..

Jacobsen, Knut Stanley, Dähnn, Michael, 2014. Statistics of ionospheric disturbances and their correlation with gnss positioning errors at high latitudes. J. Space Weather Space Clim. 4, A27. https://doi.org/10.1051/swsc/2014024..

Jakowski, N., Borries, C., Wilken, V., 2012. Introducing a Disturbance Ionosphere Index (DIX). Radio Sci. 47, RS0L14. https://doi.org/10.1029/2011RS004939.

Jakowski, N., Hoque, M., 2019. Estimation of spatial gradients and temporal variations of the total electron content using ground-based GNSS measurements. Space Weather 17. https://doi.org/10.1029/2018SW002119.

Jin, Yaqi, Moen, Jøran I., Miloch, Wojciech J., 2014. GPS scintillation effects associated with polar cap patches and substorm auroral activity: direct comparison. J. Space Weather Space Clim. 4, A23. https://doi.org/10.1051/swsc/2014019..

Jin, Yaqi, Moen, Jøran I., Oksavik, Kjellmar, Spicher, Andres, Clausen, Lasse B.N., Miloch, Wojciech J., 2017. GPS scintillations associated with cusp dynamics and polar cap patches. J. Space Weather Space Clim. 7, A23. https://doi.org/10.1051/swsc/2017022..

Johnston, G., Riddell, A., Hausler, G., 2017. The International GNSS Service. Springer International Publishing. Cham. pp. 967–982. https://doi.org/10.1007/978-3-319-42928-1..

Juan, José Miguel, Sanz, Jaume, Rovira-Garcia, Adrià, González-Casado, Guillermo, Ibáñez, D., Perez, R. Orus, 2018. AATR an ionospheric activity indicator specifically based on GNSS measurements. J. Space Weather Space Clim. 8, A14. https://doi.org/10.1051/swsc/2017044..

Jung, S., Lee, J., 2012. Long-term ionospheric anomaly monitoring for ground based augmentation systems. Radio Sci. 47. https://doi.org/10.1029/2012RS005016. https://agupubs.onlinelibrary.wiley.com/doi/abs/10.1029/2012RS005016, arXiv: https://agupubs.onlinelibrary.wiley.com/doi/pdf/10.1029/2012RS005016..

Kintner, P.M., Ledvina, B.M., de Paula, E.R., 2007. GPS and ionospheric scintillations. Space Weather 5. https://doi.org/10.1029/2006SW000260. https://agupubs.onlinelibrary.wiley.com/doi/abs/10.1029/2006SW000260, arXiv: https://agupubs.onlinelibrary.wiley.com/doi/pdf/10.1029/2006SW000260..

Klobuchar, J.A., 1987. Ionospheric time-delay algorithm for single-frequency GPS users. IEEE Trans. Aerosp. Electron. Syst. AES-23, 325–331. https://doi.org/10.1109/TAES.1987.310829.

Liu, R., Smith, P., King, J., 1983. A new solar index which leads to improved foF2 predictions using the CCIR atlas. Telecommun. J. 50, 408–414.

Liu, Y., Fu, L., Wang, J., Zhang, C., 2017. Study of GNSS loss of lock characteristics under ionosphere scintillation with GNSS Data at Weipa (Australia) during solar maximum phase. Sensors (Basel, Switzerland) 17, 2205. https://doi.org/10.3390/s17102205.

Liu, Z., Yang, Z., Xu, D., Morton, Y.J., 2019. On Inconsistent ROTI Derived From Multiconstellation GNSS Measurements of Globally Distributed GNSS Receivers for Ionospheric Irregularities Characterization. Radio Sci. 54, 215–232. https://doi.org/10.1029/2018RS006596. https://agupubs.onlinelibrary.wiley.com/doi/abs/10.1029/2018RS006596, arXiv: https://agupubs.onlinelibrary.wiley.com/doi/pdf/10.1029/2018RS006596..

Marques, Haroldo Antonio, Marques, Heloísa Alves Silva, Aquino, Marcio, Veettil, Sreeja Vadakke, Monico, João Francisco Galera, 2018. Accuracy assessment of Precise Point Positioning with multi-constellation GNSS data under ionospheric scintillation effects. J. Space Weather Space Clim. 8, A15. https://doi.org/10.1051/swsc/2017043..

van der Meeren, C., Oksavik, K., Lorentzen, D.A., Rietveld, M.T., Clausen, L.B.N., 2015. Severe and localized GNSS scintillation at the poleward edge of the nightside auroral oval during intense substorm aurora. J. Geophys. Res.: Space Phys. 120, 10607–10621. https://doi.org/10.1002/2015JA021819. https://agupubs.onlinelibrary.wiley.com/doi/abs/10.1002/2015JA021819, arXiv: https://agupubs.onlinelibrary.wiley.com/doi/pdf/10.1002/2015JA021819..

Mielich, J., Bremer, J., 2010. A modified index for the description of the ionospheric short- and long-term activity. Ann. Geophys. 28, 2227–2236. https://doi.org/10.5194/angeo-28-2227-2010. https://www.ann-geophys.net/28/2227/2010/..

Nishioka, M., Tsugawa, T., Jin, H., Ishii, M., 2017. A new ionospheric storm scale based on TEC and foF2 statistics. Space Weather 15, 228–239. https://doi.org/10.1002/2016SW001536. https://agupubs.onlinelibrary.wiley.com/doi/abs/10.1002/2016SW001536, arXiv: https://agupubs.onlinelibrary.wiley.com/doi/pdf/10.1002/2016SW001536..

Park, J., Noja, M., Stolle, C., Lühr, H., 2013. The Ionospheric Bubble Index deduced from magnetic field and plasma observations onboard Swarm. Earth Planets Space 65, 13. https://doi.org/10.5047/eps.2013.08.005..

Pi, X., Mannucci, A.J., Lindqwister, U.J., Ho, C.M., 1997. Monitoring of global ionospheric irregularities using the Worldwide GPS Network. Geophys. Res. Lett. 24, 2283–2286. https://doi.org/10.1029/97GL02273. https://agupubs.onlinelibrary.wiley.com/doi/abs/10.1029/97GL02273, arXiv: https://agupubs.onlinelibrary.wiley.com/doi/pdf/10.1029/97GL02273..

Pintor, P., Roldán, R., Gómez, J., de la Casa, C., Fidalgo, R.M., 2015. The impact of the high ionospheric activity in the EGNOS performance. Coordinates 12.

Pradipta, R., Doherty, P.H., 2016. Assessing the occurrence pattern of large ionospheric TEC gradients over the Brazilian airspace. Navigation 63, 335–343. https://doi.org/10.1002/navi.141. https://onlinelibrary.wiley.com/doi/abs/10.1002/navi.141, arXiv: https://onlinelibrary.wiley.com/doi/pdf/10.1002/navi.141..

Pullen, S., Park, Y.S., Enge, P., 2009. Impact and mitigation of ionospheric anomalies on ground-based augmentation of GNSS. Radio Sci. 44. https://agupubs.onlinelibrary.wiley.com/doi/abs/10.1029/2008RS004084. https://doi.org/10.1029/2008RS004084, arXiv: https://agupubs.onlinelibrary.wiley.com/doi/pdf/10.1029/2008RS004084..

Sieradzki, R., Paziewski, J., 2016a. MSTIDs impact on GNSS observations and its mitigation in rapid static positioning at medium baselines. Ann. Geophys. 58.

Sieradzki, R., Paziewski, J., 2016b. Study on reliable GNSS positioning with intense TEC fluctuations at high latitudes. GPS Solut. 20, 553–563. https://doi.org/10.1007/s10291-015-0466-0.

Stanislawska, I., Gulyaeva, T., 2015. Satellite Positioning. IntechOpen. chapter Ionospheric W Index Based on GNSS TEC in the Operational Use for Navigation Systems..

Tsagouri, I., Belehaki, A., Moraitis, G., Mavromichalaki, H., 2000. Positive and negative ionospheric disturbances at middle latitudes during geomagnetic storms. Geophys. Res. Lett. 27, 3579–3582. https://doi.org/10.1029/2000GL003743. https://agupubs.onlinelibrary.wiley.com/doi/abs/10.1029/2000GL003743, arXiv: https://agupubs.onlinelibrary.wiley.com/doi/pdf/10.1029/2000GL003743..

Tsagouri, I., Zolesi, B., Belehaki, A., Cander, L.R., 2005. Evaluation of the performance of the real-time updated simplified ionospheric regional model for the European area. J. Atmos. Sol.-Terres. Phys. 67, 1137–1146. https://doi.org/10.1016/j.jastp.2005.01.012. http://www.sciencedirect.com/science/article/pii/S1364682605000957. Space weather and RF communications: monitoring and modelling..

Tsagouri, I., Zolesi, B., Cander, L.R., Belehaki, A., 2010. DIAS effective sunspot number as an indicator of the ionospheric activity level over Europe. Acta Geophys. 58, 491–512. https://doi.org/10.2478/s11600-009-0045-2.

Tsai, L.C., Su, S.Y., Liu, C.H., 2016. Global morphology of ionospheric F-layer scintillations using FS3/COSMIC GPS radio occultation data. GPS Solut. 21, 1037–1048. https://doi.org/10.1007/s10291-016-0591-4.

Weber, G., Mervart, L., Stürze, A., Rülke, A., Stöcker, D., 2016. BKG Ntrip Client, Version 2.12, in: Mitteilungen des Bundesamtes für. Kartographie und Geodäsie.

Wilken, Volker, Kriegel, Martin, Jakowski, Norbert, Berdermann, Jens, 2018. An ionospheric index suitable for estimating the degree of ionospheric perturbations. J. Space Weather Space Clim. 8, A19. https://doi.org/10.1051/swsc/2018008..

Xiong, C., Stolle, C., Lühr, H., 2016. The Swarm satellite loss of GPS signal and its relation to ionospheric plasma irregularities. Space Weather 14, 563–577. https://doi.org/10.1002/2016SW001439. https://agupubs.onlinelibrary.wiley.com/doi/abs/10.1002/2016SW001439, arXiv: https://agupubs.onlinelibrary.wiley.com/doi/pdf/10.1002/2016SW001439..